MNRAS **000**, 1–17 (2011) Preprint 31 October 2019 Compiled using MNRAS LaTeX style file v3.0

TESS observations of Be stars: a new interpretation

L. A. Balona[1]* and D. Ozuyar[2]
[1] *South African Astronomical Observatory, P.O. Box 9, Observatory 7935, South Africa*
[2] *Ankara University, Faculty of Science, Dept. of Astronomy and Space Sciences, 06100, Tandogan, Ankara, Turkey*

Accepted .... Received ...

ABSTRACT

Light curves of 57 classical Be stars in *TESS* sectors 1–15 are examined. Most Be stars have structure at a fundamental frequency and one of more harmonics. In approximately 40 percent of Be stars, this structure consists of just a narrow or slightly broadened single peak. In about 30 percent of Be stars it consists of a multiple frequency group. In about 10 percent the structure is just a region of enhanced power. All these can be interpreted as non-coherent variations most likely associated with photospheric gas clouds. The harmonic structure can be used to derive approximate rotational frequencies for over 70 percent of the stars. Comparison with the projected rotational velocities shows that the photometric frequency is consistent with rotation. The first harmonic plays a prominent role in many Be stars and manifests itself in either single-wave or double-wave light curves. The reduction in amplitude of β Cep pulsations in a few Be stars during an outburst and their subsequent recovery is most likely an obscuration effect. Other instances of possible obscuration of the photosphere are suggested. A simple model, which attempts to explain these observations and other properties of Be stars, is proposed.

Key words: stars: emission-line, Be – stars: rotation – stars: oscillations

1 INTRODUCTION

The classical Be stars are dwarf and giant B stars that show, or have shown at some time, emission in the core of some Balmer lines (particularly the Hα line) (Slettebak 1979; Porter & Rivinius 2003). Stars in which the emission is a result of binary interaction are excluded from the definition. The emission is thought to be a result of mass loss from the star which is greatly assisted by rapid rotation.

In many Be stars, spectroscopic line profile and light variations characteristic of non-radial pulsation (NRP) are observed with periods of about one day. For this reason it is generally believed that NRP acts as the trigger for mass-loss outbursts which occur from time to time (Rivinius 2013). Because the additional velocity provided by NRP is relatively small, this mechanism requires the star to be rotating in excess of about 90 percent of the critical rotational velocity at the equator. In this hypothesis, every Be star must be rotating very near critical velocity.

However, it has been shown that, as a group, Be stars rotate at rates which are well below the critical rotation rate. Cranmer (2005) found that early-type Be stars have an approximately uniform spread of intrinsic rotation speed that extends from 0.4–0.6 of critical, though a few may be rotating near critical velocity. Late-type Be stars exhibit progressively narrower ranges of rotation speed as the effective temperature decreases. The lower limit rises to reach critical rotation for the coolest Be stars. More recently, Zorec et al. (2016) arrived at the same conclusion. They found that in most Be stars the ratio of equatorial rotational velocity relative to the critical rotational velocity is $v/v_c \approx 0.65$. This ratio is characterized by a wide range $0.3 < v/v_c < 0.95$, suggesting that the probability that all Be stars are critical rotators is extremely low (see also Cochetti et al. 2019).

In this paper we take the view that NRP, if present, is incidental and cannot play the main role in the mass loss mechanism. An alternative mechanism needs to be found.

It is generally accepted that early-type stars have radiative envelopes which cannot sustain magnetic fields. Therefore photospheric activity such as starspots and flares cannot exist. This has always been an important motivation for NRP as the source of mass loss in Be stars. However, recent space photometry shows that a significant fraction of A and B stars have periods which are indistinguishable from the rotational periods (Balona 2013, 2016, 2017). A study of the latest *TESS* data shows that about 35 percent of all mid- to late-B stars exhibit rotational modulation (Balona 2019). It therefore appears that starspots, or other co-rotating obscurations, may be present in many early-type stars, as they are in cooler stars. We may presume starspots, if present, are a sources of activity. Thus active regions may be the source of mass loss in Be stars.

---

* E-mail: lab@saao.ac.za

Assuming the possible presence of active regions in Be stars allows another interpretation of the line profile and light variations to be formulated. In this scenario, quasi-periodic line profile and light variation may arise not only from starspots, but perhaps also by the material ejected from these active regions.

The quasi-periodicity of many Be stars tends to cluster in two frequency groups, one twice the frequency of the other. An example of this tendency can be found in ground-based photometry of several Be stars in the open cluster NGC 3766 (Balona et al. 1991). In some seasons the fundamental group dominates and the light curve is a single wave. At other seasons the first harmonic group dominates and the light curve has a double-wave form.

Photometric observations from space have confirmed this general pattern. Examples from the *MOST* satellite include HD 163868 (Walker et al. 2005), HD 127756 and HD 217543 (Cameron et al. 2008). There are several examples from *CoRoT* as well (Neiner et al. 2009; Semaan et al. 2018). The same is found in 48 Lib observed by the *STEREO* satellite (Ozuyar et al. 2018) as do two of the three Be stars observed by *Kepler* (Rivinius et al. 2016b). These frequency groups have been interpreted as due to a large number of g-modes driven by the κ opacity mechanism. They can also be regarded as incoherent variations leading to quasi-periodicity.

In this paper we present photometric *TESS* observations of classical Be stars observed in Sectors 1–15. Observations of the most interesting stars and stars with the longest time series are presented in the main body of the text. Discussion of the remaining stars is deferred to an Appendix.

Our aim is to investigate the morphology of the light curves. Where it is possible, we attribute the frequencies or frequency groups to rotational modulation. Our aim is to test this idea by comparing the projected rotational velocity, $v \sin i$, with the equatorial rotational velocity, v, derived from the photometric frequency and the stellar radius. For this purpose we obtain stellar radius estimates using the luminosity derived from the *GAIA* DR2 parallax (Gaia Collaboration et al. 2016, 2018) and the effective temperature. If this test passes, it paves the way for a new hypothesis in which active regions may be the source of mass loss. An idea, first suggested by Balona (2003), may serve as a framework for such an hypothesis.

2 THE *TESS* DATA

The *TESS* satellite obtains precise wide-band photometry for thousands of stars with two-minute cadence in a given sector of the sky. There are 26 partially overlapping sectors and each sector is observed for approximately one month. Light curves are obtained using simple aperture photometry (SAP) and pre-search data conditioning (PDC). The PDC pipeline module uses singular value decomposition to identify and correct for time-correlated instrumental signatures in the light curves. Only PDC light curves are used in this paper. A description of how these data products were generated is provided by Jenkins et al. (2016).

It should be noted that long-term variations are difficult to correct and although PDC light curves provide the best estimate of the true light curve, unexpected deviations may occur. Note that each *TESS* pixel is 21 arcsec in size which is large, but similar to a typical aperture size used in ground-based photoelectric photometry. The chance of contamination by a star of similar brightness is therefore not negligible.

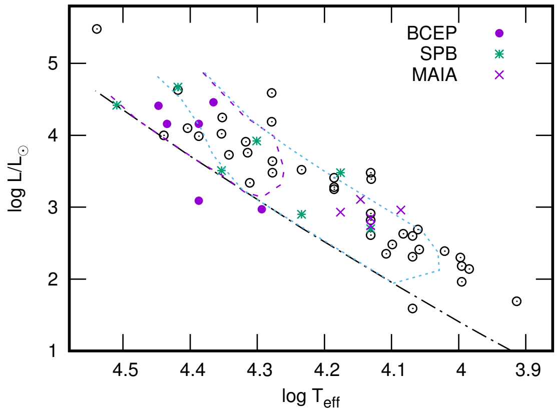

Figure 1. The H-R diagram showing the Be stars observed by *TESS*. Be stars which are also β Cep (BCEP), SPB or Maia pulsators are indicated. Also shown is the theoretical zero-age main sequence (solid line) and the instability regions of the β Cep and SPB pulsating stars.

The stars selected for analysis were chosen from the `BESS` database of classical Be stars (Neiner et al. 2011) and observed in quarters 1–15. These are shown in Table 1. The *TESS* input catalogue (Stassun et al. 2018) lists stellar parameters for stars observed by *TESS*. The effective temperatures, $T_{\rm eff}$, of Be stars are poorly known because the line blanketing caused by circumstellar material leads to unreliable estimates from multicolour photometry. For this reason, the effective temperatures used in this paper are, whenever possible, from spectroscopic modelling. Failing this, they are estimated from the spectral type and luminosity class using the calibration of Pecaut & Mamajek (2013). The error in $T_{\rm eff}$, as estimated from the dispersion in spectral types, is about 1000 K.

Stellar luminosities were derived from *GAIA* DR2 parallaxes (Gaia Collaboration et al. 2016, 2018). The bolometric correction was obtained from $T_{\rm eff}$ using the calibration of Pecaut & Mamajek (2013). The reddening correction was derived from a three-dimensional reddening map by Gontcharov (2017). The formal error in luminosity, $\log L/L_\odot$, as estimated from the error in the parallax, bolometric correction and extinction, is about 0.05 dex, but in reality is likely to be larger. The theoretical H–R diagram is shown in Fig. 1, showing that the stars are equally distributed between early and late B stars.

The projected rotational velocities in Table 1 are mostly from the catalogue of Glebocki & Gnacinski (2005) supplemented by more recent measurements when available. The typical error in $v \sin i$ for B stars can be estimated from the catalogue. The error increases with $v \sin i$ and ranges up to 60 km s^{-1}. A representative value of $\sigma_{v \sin i} = 30\,{\rm km\,s^{-1}}$ is assumed. From the error in $\log L/L_\odot$ and $T_{\rm eff}$ it is easy to calculate the error in the derived stellar radius and hence the equatorial rotational velocity, v, deduced from the photometric rotational frequency, $\nu_{\rm rot}$. This error depends almost

Table 1. List of Be stars selected for analysis. The *TESS* catalogue number, TIC, and the HD number are listed. This is followed by the variability classification based purely on the *TESS* light curve. The number of *TESS* sectors is given by N. The V magnitude, the effective temperature, $T_{\rm eff}$ (K), and the literature reference for $T_{\rm eff}$ are given. The stellar luminosity determined from the *GAIA* parallax is shown and is followed by the projected rotational velocity, $v\sin i$ (km s^{-1}). The last column gives the spectral classification.

TIC	HD	Var Type	N	V	$T_{\rm eff}$	Ref	$\log \frac{L}{L_\odot}$	$\nu_{\rm rot}$	v	$v\sin i$	Sp Type
23037766	57150	ROT	1	4.670	22000	2	3.73	1.07	270	210	B2V + B3IVne
42360166	191610	BE/ROT?	2	4.930	20470	9	3.34	1.5	280	320	B2.5III
47296054	214748	ROT	1	4.180	11500	2	2.69	0.836	240	180	B8/9IV/V
52665242	47054	ROT	1	5.520	13520	1	2.91	1.145	300	260	B8IV/Ve shell
53992511	209522	SPB+ROT	1	5.952	22570	1	3.51	1.6	300	280	B3V + B:
55295028	33599	ROT+BCEP	13	8.970	23200	7	4.46	0.905	480	200	B3p shell
56179720	30076	SPB	1	5.810	26190	1	4.67	-	-	180	B1V?e
65803653	56014	BCEP+ROT	1	4.650	24380	1	4.16	1.3	440	210	B2V(e) shell
67251066	198183	BE/ROT?	1	4.540	15330	1	3.25	1.1	330	120	B7.5IV
71132174	28497	SPB+ROT	1	5.410	32310	9	4.42	1.4	370	230	B1Ve
71727949	41335	-	1	5.210	22500	2	4.25	-	-	340	B1:IV/V:nne shell
75047606	79621	ROT?	2	5.920	11710	1	2.31	1.67	290	170	B9V
81584371	54309	ROT?	1	5.830	26190	1	4.63	0.75	380	200	B1.5III
99115271	193911	ROT	1	5.560	15330	1	3.41	0.529	190	200	B7IV/Ve shell
120967488	178475	ROT?	1	5.249	18950	1	3.48	1.0	260	230	B5/8
139385056	58978	BCEP	1	5.560	28000	1	4.41	-	-	280	B0.5IVn(e)p
139472176	14850	ROT	1	8.400	13500	7	3.39	0.773	350	200	B7III/IVe
140214221	37795	ROT	2	2.652	12200	2		1.841		180	B7IVe
144028101	135734	MAIA	1	4.274	13520	1		-		279	B8Ve
148316007	49319	BCEP+ROT	2	6.625	24380	1	3.09	2.5	400	245	B2/3IVne
148917425	109387	MAIA+ROT	2	3.890	14000	6	3.11	0.882	270	200	B6III(n)
151300497	155806	-	1	5.530	34600	1	5.48	-		115	O7.5V((f))z(e)
159117671	112028	ROT+ROT	1	5.350	9650	1	2.14	1.252	270	200	A1IIIp shell
174664153	61925	ROT	2	6.004	22570	1	4.02	1.019	350	200	B3IV(e);
175523591	63215	SPB/ROT?	2	5.870	17140	1	2.90	2.5	400	271	B6Vnn
195744427	199629	ROT?	1	3.940	9900	1	1.96	-		219	A0.5IIIn
207176480	19818	ROT+FLARE	2	9.060	11710	1	1.59	0.298	90		B9/A0Vne:
230981971	10144	(SPB/ROT	1	0.460	15000	8	3.48	0.75	350	260	B4V(e)
234230792	49330	BCEP+ROT	1	8.950	27200	7	4.16	1.47	400	200	B0:nnep
245286665	192044	ROT	1	5.920	15330	1	3.28	1.039	330	280	B7IV/V:ne shell
258704817	129954	-	1	5.880	24380	1	3.99	-	-	180	B2.5V
259449942	60855	EB:/ROT	1	5.700	20760	1	3.91	1.1	390	230	B4III:n shell
260640910	46860	SPB+ROT	12	5.707	13520	1	2.70	1.392	290	200	B8III
270219259	209014	MAIA	1	5.620	12200	1	2.96	-	-	350	B8III shell
277103567	37935	ROT	3	6.281	9940	5	2.30	1.497	360	209	B9.5V
279430029	53048	ROT	13	7.920	18950	1	3.64	1.784	550		B5/7Vn(e:)
281741629	CD-56 152	-	1	10.180	19000	4	4.59	-	-	180	sdB?/Be?
296969980	131492	SPB	1	5.110	20000	2	3.92	-	-	100	B2IV/V
302962039	78764	-	4	4.654	19000	2	4.19	-		140	B2IV:n(e) He-s
308748912	68423	-	6	6.313	12100	2	2.63	-	-	26	B7IVek;
334776134	91120	ROT	1	5.580	11453	10	2.41	1.3	270	250	B9IV/V shell
341040849	64831	ROT	4	7.830	13520	1	2.61	1.406	260		B8Vn(e)
355653322	224686	ROT	1	4.470	10500	2	2.39	1.266	300	275	B9IIIn
358467471	65663	-	5	6.741	13520	1	3.48	-		120	B8IIIe
363748801	149671	ROT	1	5.882	13520	1	2.82	1.555	370	230	B8:V:
364398342	66194	ROT	7	5.810	20632	3	3.76	1.25	380	200	B2IVn(e)p(Si)
405520863	110335	ROT	1	4.940	17140	1	3.52	1.298	430	244	B6IVe
408382023	83953	MAIA+ROT	1	4.760	15000	2	2.93	1.55	340	260	B6V(e)
409358619	124367	BCEP+ROT	1	5.070	19650	2	2.97	2.768	370	280	B5:Vnne
423528378	107348	ROT	1	5.210	12830	2	2.35	2.306	350	250	B8Vn
425224332	58715	ROT	1	2.890	12560	11	2.48	1.61	300	260	B8IV/Ve shell
427395049	37041	-	1	6.390	27500	2	4.00	-	-	130	O9.5Vpe
439397894	225132	ROT	1	4.543	9900	1	2.18	1.441	300	211	A0:IV
443616529	98058	DSCT	1	4.467	8200	2	1.69	-		230	A7IV shell
452163402	100673	ROT?	1	4.614	11710	1	2.60	1.364	330	125	B9V(e?)
463103957	88661	ROT?	2	5.750	25350	9	4.10	1.36	400	220	B2IVnep
469421586	195554	MAIA+ROT	1	5.889	13520	1	2.85	1.66	400	240	B8IV/V

References to $T_{\rm eff}$:
1 - MK Type (Pecaut & Mamajek 2013); 2 - Arcos et al. (2018); 3 - Silaj & Landstreet (2014); 4 - Silva & Napiwotzki (2011);
5 - Balona (1994); 6 - Saad et al. (2004); 7 - Levenhagen & Leister (2006); 8 - Domiciano de Souza et al. (2014);
9 - Zorec et al. (2016); 10 - Shokry et al. (2018); 11 - Harmanec et al. (2019).

entirely on the error in $T_{\rm eff}$. The contribution from the luminosity error is small while the contribution from the error in the presumed rotational frequency is negligible. The typical value for the error in the derived equatorial rotational velocity is $\sigma_v \approx 40\,{\rm km\,s^{-1}}$.

2.1 Photometric Data and Analysis

To detect periodic stellar signals, the Lomb-Scargle (Lomb 1976; Scargle 1982) technique is used. Details related to the production of amplitude spectra and the calculation of the significance levels can be found in Balona (2014). The frequencies and amplitudes can be classically represented in two ways: the time-domain and the frequency-domain representations (Boashash 2015). However, the power spectrum does not provide information related to changes of frequency and amplitude with time. Such information may be very important in diagnosing the source of the variation and are best represented by a time-frequency diagram (Boashash 2015).

In obtaining the time-frequency diagram, the Lomb-Scargle periodogram was calculated in a fixed time window. The length of the window was chosen to be five days as a compromise between a good signal-to-noise ratio and reasonable frequency resolution. The window is shifted with a time step of 0.5 d. At each time step, the periodogram (amplitude vs frequency) is plotted. In the resulting time-frequency diagram, the amplitude is coded by color or grey level.

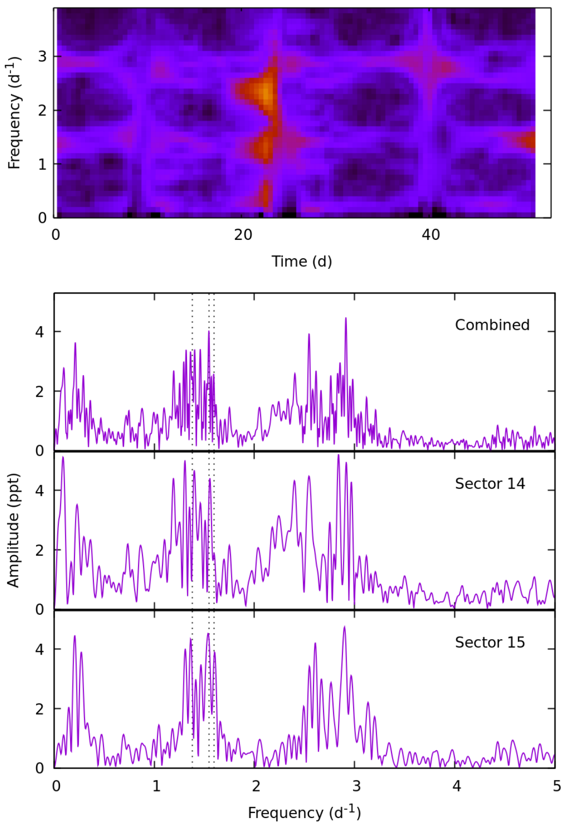

Figure 2. Time-frequency diagram and periodograms of the combined data and of individual observing sectors of TIC 42360166 (28 Cyg). The vertical dotted lines represent the frequencies 1.381, 1.545 and 1.597 d^{-1} mentioned by Baade et al. (2018b).

3 VARIABILITY CLASSIFICATION

In the *General Catalogue of Variable Stars* (GCVS, Samus et al. 2017), the variability type BE is used for Be stars with mild to moderate light outbursts. The GCAS (γ Cas) type is used for eruptive early Be stars where outbursts may exceed 1 mag. These variations refer to the effects of the outburst itself and to circumstellar material on the light curve. There is no GCVS classification for hot rotational variables other than those with chemical peculiarities. For this reason, the ROT class was introduced. For a brief discussion on classification of variable stars see Balona et al. (2019).

While starspots may be present in Be stars, and may be detected in the light curve, circumstellar material is an important contribution to the light variation. The tentative framework that we adopt in describing the quasi-periodic light variations in Be stars is that these are a result of co-rotating gas clouds ejected by active regions associated with starspots, rather than the starspots themselves. They therefore give rise to incoherent light variations with a quasi-period close to the rotation period of the star. In the periodogram this manifests as groups of peaks or broad humps of power at the approximate rotational frequency and its harmonic.

One also needs to bear in mind that NRP will occur in some Be stars. The Be stars lie in either, or both, the β Cep or SPB instability strips. Some stars have high frequencies, but are too cool to be classified as β Cep and too hot for δ Scuti. These are classified as Maia variables (Balona et al. 2016). It is very easy to identify β Cep or Maia Be stars because of the high frequencies. It is more difficult to distinguish SPB stars from rotation modulation as the frequency range overlaps. The criterion used in that if harmonics are present then rotation cannot be excluded and the ROT class is applied. From the fundamental photometric frequency, the equatorial rotational velocity is estimated. This will be compared with $v \sin i$ as a consistency test.

4 RESULTS

There are several stars where *TESS* observations cover many sectors. These are of particular interest as it allows exploration of how the star behaves over a period of many months. Certain well-observed stars are also of interest even if the observations are only from one sector. These stars are discussed below. The remaining stars, nearly all of which were observed in only one sector, are discussed in the Appendix.

4.1 TIC 42360166, 28 Cyg

Spectroscopic observations of 28 Cyg have generally confirmed the presence of a group of frequencies at around 1.56 d^{-1} (Peters & Penrod 1988; Pavlovski & Ruzic 1990; Hahula & Gies 1994) and also around 1.4 d^{-1} (Spear et al. 1981; Bossi et al. 1993). Tubbesing et al. (2000) confirmed the 1.56 d^{-1} frequency and found another group at about 1.60 d^{-1}. 28 Cyg was extensively studied by Baade et al.

Table 2. Extracted frequencies, ν (d^{-1}), and amplitudes, A (ppt). The figures in brackets denote the error in the last digit.

ν	A	ν	A	ν	A
TIC 55295028:					
0.13153(2)	2.18(1)	0.95524(1)	3.38(1)	2.87294(3)	0.58(1)
0.45470(3)	0.71(1)	1.68398(3)	1.01(1)	3.26101(3)	0.45(1)
0.74254(2)	0.94(1)	1.74804(2)	1.15(1)	3.42813(4)	0.37(1)
0.77574(2)	1.38(1)	1.77917(2)	1.47(1)	3.77002(4)	0.41(1)
0.87502(1)	4.39(1)	1.91077(1)	2.02(1)	3.93364(5)	0.24(1)
0.90312(2)	1.55(1)	2.84010(3)	0.77(1)	5.17140(3)	0.47(1)
TIC 65803653 (27 CMa):					
0.7896(4)	2.09(1)	2.6793(4)	1.54(1)	13.1131(9)	0.10(1)
1.2608(4)	2.06(1)	5.1578(6)	0.35(1)	13.5096(5)	0.54(1)
1.3472(4)	1.68(1)	5.9020(7)	0.31(1)	14.7340(9)	0.11(1)
1.4060(4)	1.26(1)	10.8837(4)	1.08(1)	24.3903(9)	0.09(1)
2.6240(4)	1.88(1)				
TIC 234230792 (HD 49330):					
0.8601(7)	1.56(3)	2.9164(4)	3.34(3)	5.8908(9)	0.83(3)
2.4565(8)	1.31(3)	4.2518(7)	1.48(3)	11.8657(9)	0.77(3)
2.6044(7)	1.66(3)	4.3771(9)	0.85(3)	16.1122(9)	0.27(3)
2.7154(7)	2.39(3)				

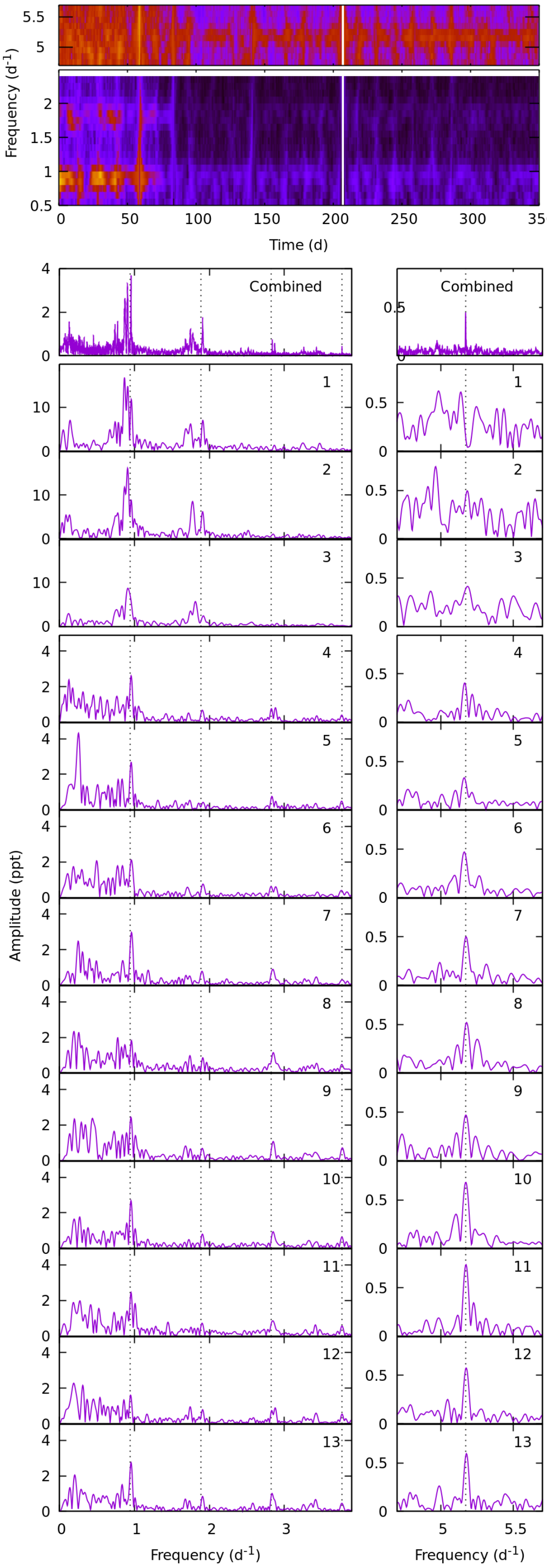

Figure 3. The time-frequency diagram and periodograms of the combined data and of individual observing sectors (labeled) of TIC 55295028. Note the changes in amplitude scale in the periodograms. The vertical dotted lines represent the frequency $\nu = 0.94\,\mathrm{d}^{-1}$ and its three harmonics on the left. The right hand panels shows the peak $\nu = 5.17141\,\mathrm{d}^{-1}$.

(2018b) using photometric data from the *BRITE* and *SMEI* satellites. The variability is clustered into three frequency groups with approximate ranges 0.1–0.5, 1.0–1.7 and 2.2–3.0 d^{-1}. The peaks of highest amplitude occur at 1.381, 1.545 and 1.597 d^{-1}.

Baade et al. (2018b) note that stochastic variability is an important contribution to the light curve. However, they stress that coherent variations certainly occur and that Be stars are not erratic or even chaotic variables. They point out the clear signature of low-order g-mode pulsations in high-resolution spectra (Rivinius et al. 2003), demonstrating coherent, and coherently varying, large-scale structures in the photosphere. These observations were, necessarily, of relatively short duration so it is not entirely clear that coherence is well established.

Periodograms of the *TESS* data are shown in Fig. 2. These look very different from the *BRITE* periodograms in that the frequency spectrum is much denser. However, the two groups around 1.0–1.7 and 2.2–3.0 d^{-1} are still present. The three coherent peaks of largest amplitude mentioned by Baade et al. (2018b) do not agree with peaks in the *TESS* data. Either the amplitudes are lower or the frequencies are not quite as coherent as expected. Note that peaks in sector 14 look quite different from those in sector 15 and that the time-frequency diagram suggests somewhat erratic behaviour.

Because one frequency group is roughly twice the frequency of the other, we have assumed that the fundamental group at around 1.5 d^{-1} reflects the approximate rotational frequency of the star.

4.2 TIC 55295028, HD 33599

Bernhard et al. (2018) detected a frequency of 0.9051 d^{-1} from ground-based photometry. Balona et al. (2019) did not detect a period from *TESS* sector 1–2.

The time-frequency diagram (Fig 3) shows two groups with fundamental frequency of around 0.94 d^{-1} which we adopt as the rotational frequency. Three harmonics are visible as indicated by the dotted lines, although only the first is of moderate amplitude. There is a sudden decline in am-

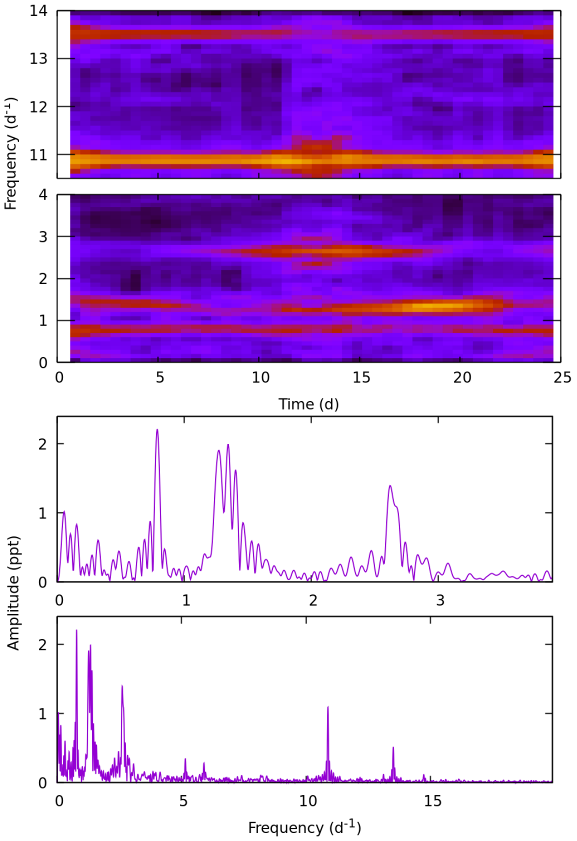

Figure 4. Time-frequency diagrams and periodograms of TIC 65803653 (27 CMa) showing high frequencies as well as variable-amplitude peaks.

plitude in all groups between sector 3 and 4. Rapid changes in amplitude, and equally rapid recovery, seem to be visible in a few stars (see below).

There is also a low-amplitude peak at $5.171\,\mathrm{d}^{-1}$ which is first visible in sector 4 and subsequent sectors. The line is sharp and the frequency constant (right panel in Fig. 3). It does not seem to be harmonically related to the broad peak groups and is most probably due to pulsation. The star may thus be classified as a β Cep variable. Extracted frequencies are listed in Table 2. It is possible that the β Cep pulsation retains constant amplitude, but the increased background noise in sectors 1–3 renders it less visible.

4.3 TIC 65803653, 27 CMa

27 CMa is a very close optical multiple system. From ground-based photometry, Balona & Rozowsky (1991) found a single frequency, $0.7925\,\mathrm{d}^{-1}$, in 1986 and 1987. When the star was next observed in 1990, in addition to the quoted frequency, a new peak at $10.8914\,\mathrm{d}^{-1}$ made its appearance. The high frequency, characteristic of a β Cep star, was still present in 1991.

The appearance of β CMa pulsations may be related to the changes in the spectrum reported by Bhattacharyya & Ghosh (1989) and Ghosh et al. (1989). Prior to the appearance of β Cep pulsations, observations showed typical double-peaked Hα emission. In 1989, Apr 16–26 the Hα and HeI 5876 lines displayed P-Cyg profiles. By 1989, Oct 14–15 the appearance of the spectrum in the region of Hα, Si 6347, Si 6371 and HeI 5876 suggested that the star had entered into a shell phase when compared to the previous observations in April.

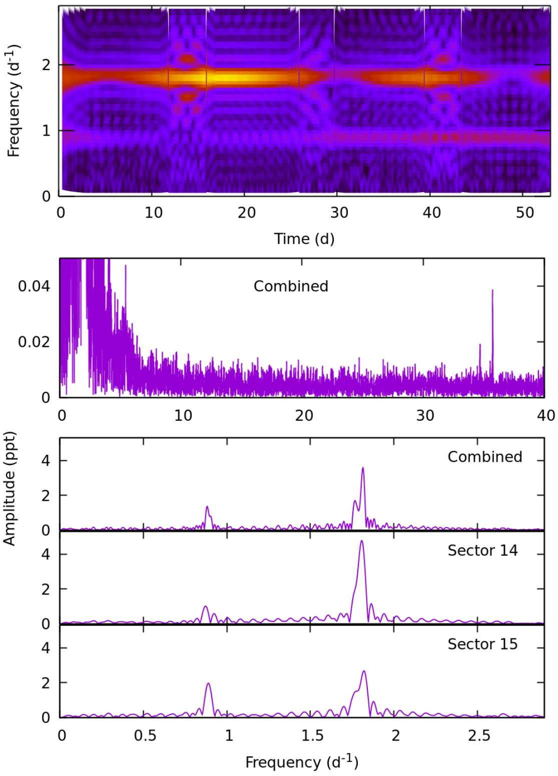

Figure 5. Time-frequency diagram and periodograms of TIC 148917425 (κ Dra) showing high frequencies (top panel) as well as variable-amplitude rotational peaks.

Since self-driven pulsations are not known to appear and disappear in non-Be stars, it is perhaps possible that the pulsations were simply masked from view during the development of the shell phase. Once the shell phase was established, the obscuration was removed and the β Cep pulsations became visible.

The *TESS* periodogram (Fig. 4) shows multiple peaks in which β Cep pulsations are visible. A list of extracted frequencies is shown in Table 2. The peak at $10.8837\,\mathrm{d}^{-1}$ corresponds to that seen by Balona & Rozowsky (1991). The time-frequency diagram indicates variability in both amplitude and frequency in some of the low-frequency peaks. By contrast, the frequency and amplitude of the β Cep pulsations seem to be stable. The peak at $2.6\,\mathrm{d}^{-1}$ seems to be an harmonic of the broad peak at around $\nu = 1.3\,\mathrm{d}^{-1}$ which is assumed to be the rotational frequency. The nature of the $0.7896\,\mathrm{d}^{-1}$ frequency, which is the one observed by Balona & Rozowsky (1991), is not clear. It appears to be stable in both frequency and amplitude.

4.4 TIC 148917425, κ Dra

Baker (1920) found κ Dra to be a spectroscopic binary with a period of 8.986 d. Later Hill (1926) confirmed the binary nature but with a period of 0.89038 d which is the 1-d alias of the former period. Juza et al. (1991) obtained further spectroscopic observations and confirmed the presence of the 0.89-d period which is transient in nature and suggested that it might be the rotation period. In addition, they found the star to be a binary with a period of 61.55 d.

The *TESS* time-frequency diagram (Fig, 5) shows two frequencies which appear to be variable in amplitude. The periodograms show a pair of high-frequency peaks at 34.696 and 35.744 d^{-1} (amplitudes 0.019 and 0.040 ppt). This would suggest that it is a Maia star (Balona et al. 2016) since it is too cool for a β Cep variable. The high frequencies might also be explained as originating in a δ Scuti companion. There are also two broad peaks with multiple structures at a frequency of $\nu \approx 0.89\,\mathrm{d}^{-1}$ and its harmonic (amplitudes about 1.4 and 3.7 ppt respectively) which change amplitude. This is not the spectroscopic frequency, $1.12\,\mathrm{d}^{-1}$ found by Juza et al. (1991), but another 1-d alias. Note that the first harmonic has larger amplitude than the fundamental. The light curve will thus be of the double-wave kind.

4.5 TIC 207176480, HIP 14595

Houk & Cowley (1975) classified (HD 19818) as B9/A0Vne: with weak Balmer emission. It is an X-ray source (Naze & Motch 2018). From ground-based *KELT* photometry, Oelkers et al. (2018) obtained a frequency of $0.7031\,\mathrm{d}^{-1}$.

Balona et al. (2019) list the star, but no periodicity was found from *TESS* sector 2 alone. The additional sector 3 observations show two strong flares at BJD 2458377.72 and BJD 2458393.80 (Fig. 6). These are probably related to the X-ray source. On removing the flares, the resulting periodogram shows just a single peak at $0.2977\,\mathrm{d}^{-1}$ (amplitude 2.740 ppt) which may be the rotational frequency. It may also represent an orbital frequency in which the secondary is involved in generating the X-rays and flares. The *KELT* frequency is the 1-d alias of the true frequency. The projected rotational velocity is not known. It would be important to obtain more detailed spectroscopic observations of this interesting star.

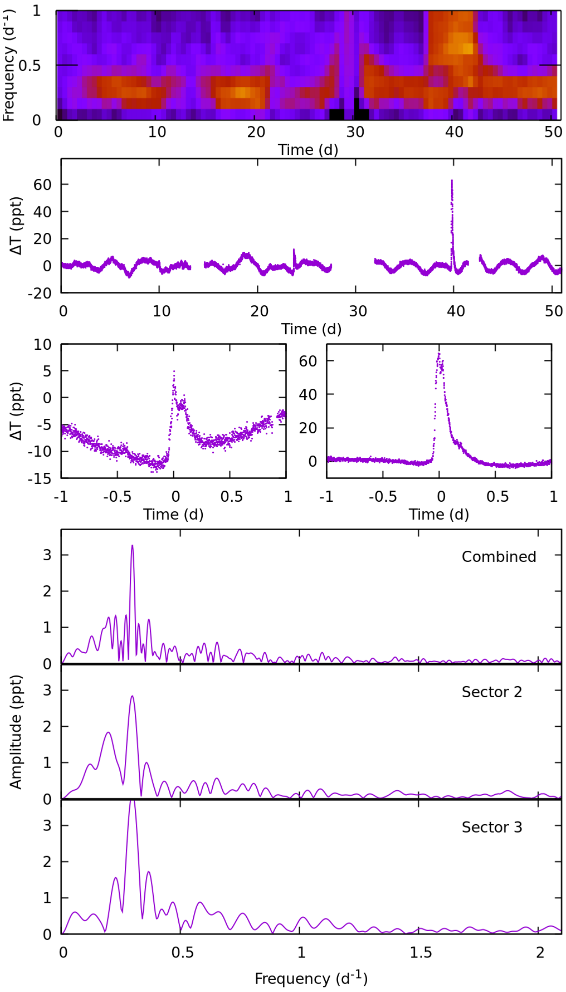

Figure 6. The top panel is time-frequency diagram of TIC 207176480 (HD 19818) showing amplitude changes in the $0.2977\,\mathrm{d}^{-1}$ frequency. The next three panels show the light curve and detail of two flares. The bottom three panels show periodograms of the combined data and periodograms of data in two sectors.

4.6 TIC 230981971, α Eri

Achernar (HD 10144) is the brightest and the nearest Be star in the sky. Using Earth-rotation synthesis on the *VLT* interferometer Domiciano de Souza et al. (2003) measured an oblateness of 1.56 ± 0.05. The star has a close companion, most likely an A1V–A3V star, with an orbital period of about 15 yr (Kervella et al. 2008). The first indication of short-period variations was a photometric/spectroscopic study by Balona et al. (1987) who found a frequency of $0.79\,\mathrm{d}^{-1}$. From line profile observations, Rivinius et al. (2003) found a frequency of $0.77\,\mathrm{d}^{-1}$. Goss et al. (2011) used photometry from the *SMEI* instrument obtained in yearly 50-d segments over a 5-yr period. They found frequencies of 0.725, 0.775 and one of much lower amplitude at $0.689\,\mathrm{d}^{-1}$, all with variable amplitudes. The $0.775\,\mathrm{d}^{-1}$ frequency appears to be coherent over the whole period, while the $0.725\,\mathrm{d}^{-1}$ frequency did not exhibit coherence. Balona et al. (2019) did not detect a period from *TESS* sectors 1–2.

The periodogram from one sector of *TESS* observations show two peak groupings at around 0.73 and $1.46\,\mathrm{d}^{-1}$. Each group shows multiple closely-spaced peaks (Fig. 7). The *TESS* periodogram is very similar to the one obtained by Goss et al. (2011) and the frequencies at 0.725 and $0.775\,\mathrm{d}^{-1}$ seem to be still present (dotted lines in the figure). Judging from the time-frequency diagram, amplitude variations are present in both frequency groups. The peaks at $1.45\,\mathrm{d}^{-1}$ also appear to change frequency.

Domiciano de Souza et al. (2014) derive the stellar parameters from interferometric observations, finding an equatorial radius $R_{\mathrm{eq}} = 9.16 \pm 0.20 R_{\odot}$. They adopt $0.689\,\mathrm{d}^{-1}$ as the rotational frequency, which is the lowest-amplitude frequency found by Goss et al. (2011), because it fits better with their calculations. This leads to $v/v_c \approx 0.81$. If we assume that $0.73\,\mathrm{d}^{-1}$ represents the rotational frequency (with the $1.46\,\mathrm{d}^{-1}$ the first harmonic), an equatorial rotational velocity of $340\,\mathrm{km\,s}^{-1}$ and $v/v_c \approx 0.74$ is obtained

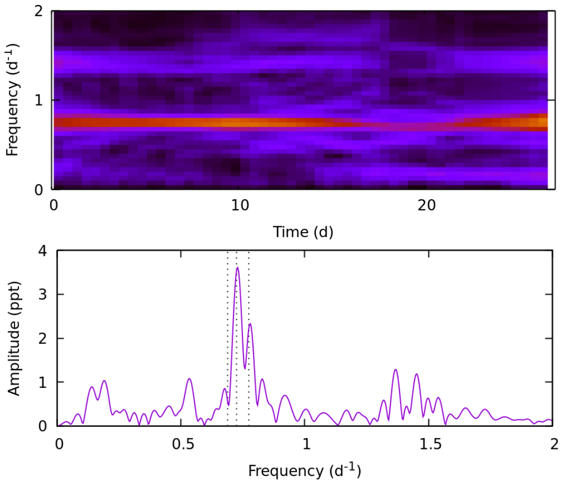

Figure 7. The top panel shows the time-frequency diagram of TIC 230981971 (α Eri) from *TESS* sector 2 data. The bottom panel is the corresponding periodogram. The dotted lines are the frequencies 0.689, 0.725 and 0.775 d^{-1} found by Goss et al. (2011).

using $R_{\rm eq} = 9.16 R_\odot$. The projected rotational velocity is $v \sin i = 260 \pm 15\,{\rm km\,s^{-1}}$ (Domiciano de Souza et al. 2014).

The actual $v \sin i$ of Achernar seems to significantly vary in time, as shown by Rivinius et al. (2013). The reported values span the range 223–290 km s^{-1}. The value appears to correlate with the disk emission, being higher at when emission is strongest. It is interpreted as a variation of the equatorial rotation rate of photospheric layers and further elaborated by Rivinius et al. (2016a).

4.7 TIC 234230792, HD 49330

HD 49330 was observed by the *CoRoT* mission for nearly 137 d during 2007–2008 with a time sampling of 1 s as described by Huat et al. (2009). During this time the star underwent a mini outburst where the brightness increased by 0.03 mag over the course of 20 d (Fig. 8). In Be stars, a major outburst can lead to a brightness change of several tenths of a magnitude in just a few days. Prior to, during, and after the outburst, Huat et al. (2009) identify four phases as shown in Fig. 8. The periodogram of the *TESS* data, also shown in the figure, closely resembles the outburst phase. Extracted frequencies are listed in Table 2.

During the precursor and outburst phases two groups of peaks around 1.47 and 2.94 d^{-1} gradually emerge. In addition, a more concentrated group around 0.87 and 1.28 d^{-1} also makes its appearance. The amplitudes of the high-frequency β Cep pulsations at 11.86 and 5.03 d^{-1} decrease remarkably during the outburst phase.

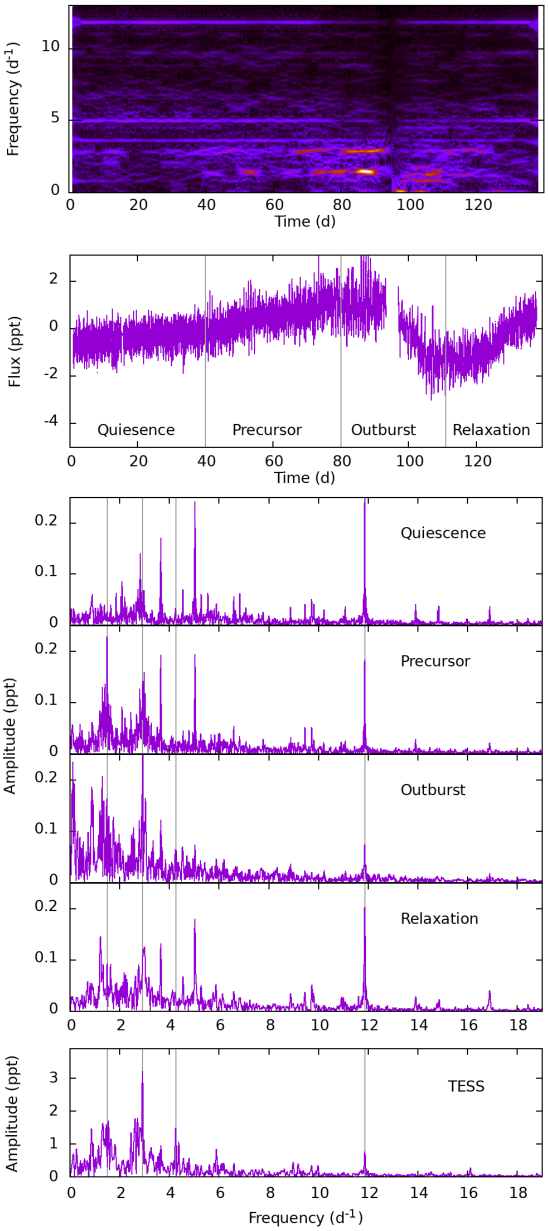

Figure 8. The top panel is the time-frequency diagram for *CoRoT* observations of TIC 234230792 (HD 49330). Below this is the *CoRot* light curve showing four phases of the mini-outburst. Below this panel, the *CoRoT* periodograms corresponding to each outburst phase are shown. The bottom panel is the *TESS* sector 6 periodogram. The dotted lines are frequencies 1.4934, 2.9164, 4.2518 and 11.8657 d^{-1}.

Huat et al. (2009) interpret the peak groups around 1.47 and 2.94 d^{-1} as systems of closely-spaced g modes. They find a correlation between both amplitude changes and the presence/absence of certain frequencies of pulsations at the different phases of the outburst. The amplitudes of the main frequencies (the β Cep modes) decrease before and during the outburst and increase again after the outburst. Also, several groups of frequencies (g modes) appear just before the outburst, reach maximum amplitude during the outburst and then disappear as soon as the outburst has finished. As already mentioned, these are interpreted as g modes with short lifetimes. They suggest that the frequency group around 0.87 d^{-1}, which is compatible with the rotational frequency, could be explained by the ejection of material co-rotating with the star.

The interpretation by Huat et al. (2009) is in line with the common view that NRP is the cause of the mass loss (Rivinius et al. 1998). The idea is that the sudden large increase in mode amplitudes of the groups around 1.47 and

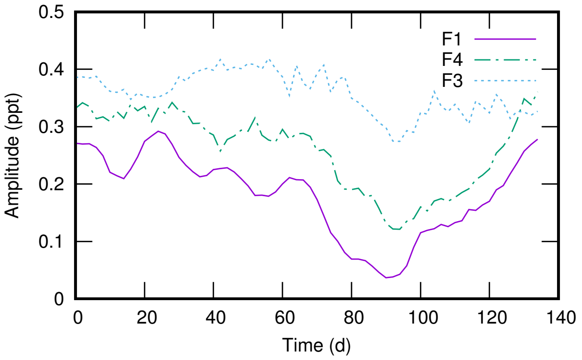

Figure 9. Variation of the amplitudes of the β Cep modes with frequencies $F1 = 11.8639$, $F3 = 3.6594$ and $F4 = 5.0260\,\mathrm{d}^{-1}$ as a function of time from the *CoRoT* data of HD 49330. The amplitudes have been arbitrarily displaced to reduce confusion.

$2.94\,\mathrm{d}^{-1}$ is responsible for the ejection of material. The decrease in amplitude shortly afterwards shuts off further mass loss. However, Huat et al. (2009) also point out that it is the occurrence of the outburst that might lead to the excitation of different modes, and not the converse.

In our view, both these interpretations are not consistent with the available information. In the first place, it is clear that Be stars, in general, do not rotate very close to the critical rotation rate, as required by the notion that pulsation acts as a trigger for mass loss. Also, the so-called g-mode groups around 1.47 and $2.94\,\mathrm{d}^{-1}$ appear to be non-coherent as is evident from the time-frequency diagram of Fig. 8. Note the appearance of these frequency groups compared to the smooth appearance of the β Cep pulsations at 3.6594, 5.0260 and $11.8639\,\mathrm{d}^{-1}$. Finally, no pulsating star so far observed shows such rapid increase and decrease of pulsation amplitudes. Amplitude changes in all known self-excited pulsating stars occur over timescales of months to years and never in just a few days.

An alternative interpretation that may be considered is that there is an active region on the star which is responsible for driving mass loss. The ejected gas clouds obscure light and results in rotational light modulation. We can identify the rotational frequency as approximately $1.47\,\mathrm{d}^{-1}$ with $2.94\,\mathrm{d}^{-1}$ being the harmonic (and not an independent group of g modes). The rapid increase of amplitude of these two frequencies is caused by the build-up of ejected material co-rotating with the star. The ejected material masks the photosphere, resulting in a decrease of visibility of the β Cep pulsations during the outburst. As the material disperses, the photosphere and the β Cep pulsations regain their original amplitudes.

That the decrease in pulsation amplitude of the β Cep modes is an obscuration effect is demonstrated by the variation of the pulsation amplitudes with time for the modes at 3.6594, 5.0260 and $11.8639\,\mathrm{d}^{-1}$. The amplitudes of these modes vary in exactly the same way with time as can be seen in Fig. 9. This is extremely unlikely to occur in the NRP interpretation because this requires that three independent modes, which are bound to have different growth rates, change amplitude by the same fraction as a function of time.

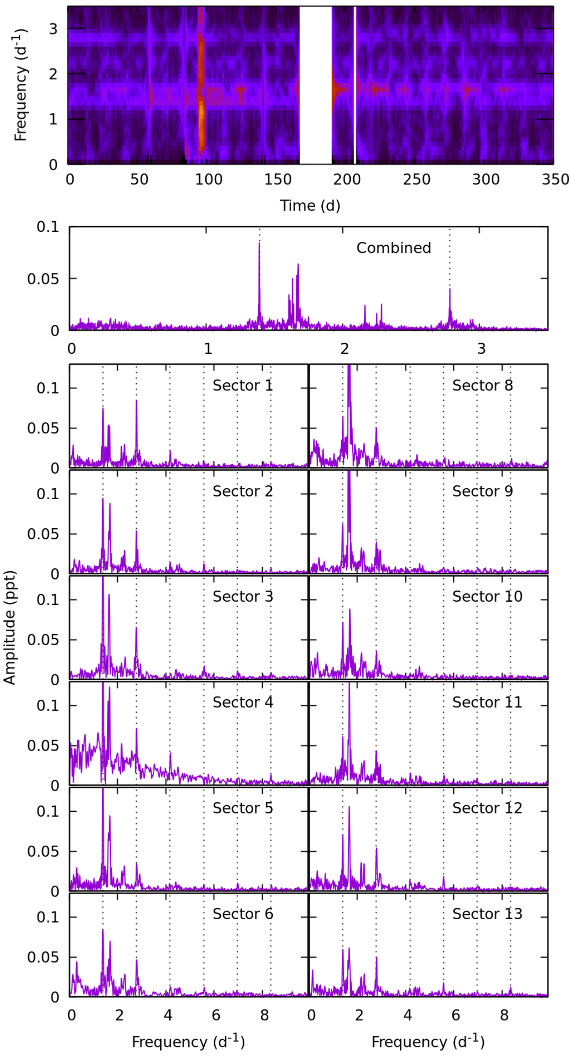

Figure 10. Time-frequency diagram and periodograms of the combined data and of individual observing sectors of TIC 260640910 (μ Pic). The dotted lines show $nu = 1.38854(1)\,\mathrm{d}^{-1}$ and 5 harmonics.

4.8 TIC 260640910, μ Pic

The shell star μ Pic is a double star (B9IVn + A8V:p) with a separation of 2.4 arcsec and a magnitude difference of 3.2 mag. Balona et al. (1992) found a frequency of $2.52\,\mathrm{d}^{-1}$ from ground-based photometry. The first two *TESS* sectors were analysed by Balona et al. (2019), but no periodicity was found.

The periodogram of all 12 sectors (Fig. 10) shows multiple peaks characteristic of an SPB pulsating variable. The main peak at $1.392\,\mathrm{d}^{-1}$ (amplitude 0.08 ppt) appears to be slightly broadened or double and of variable amplitude. This does not bear any relationship to the frequency mentioned by (Balona et al. 1992). Up to 5 harmonics are visible as shown in Fig. 10, each harmonic being rather broad. This may be the rotational frequency. A secondary peak system at about $1.63\,\mathrm{d}^{-1}$ consists of multiple peaks of variable am-

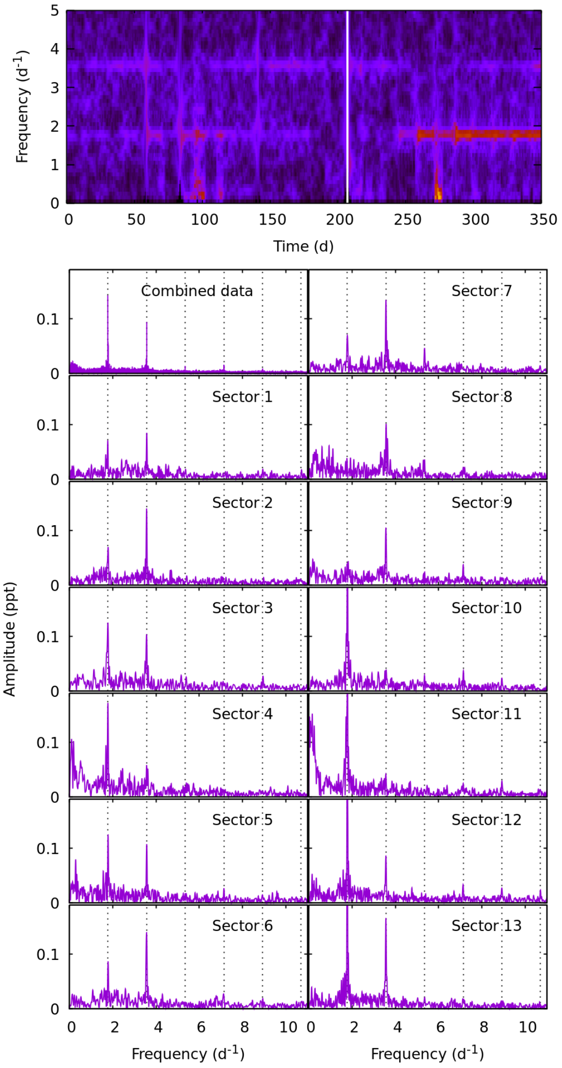

Figure 11. Time-frequency diagram and periodograms of the combined data and of individual observing sectors of TIC 279430029. The vertical dotted lines represent the frequency $\nu = 1.784\,\mathrm{d}^{-1}$ and its harmonics.

plitude which may be due to g-mode pulsations. For this reason we classify the star as SPB+ROT.

4.9 TIC 279430029, HD 53048

Balona et al. (2019) found a frequency of $1.784\,\mathrm{d}^{-1}$ and its harmonic from first-light *TESS* observations. The periodogram of the complete data set (13 sectors) confirms a broad or unresolved main peak at this frequency with amplitude of 0.14 ppt. Five harmonics are visible and we assume $1.784\,\mathrm{d}^{-1}$ to be the rotational frequency. The amplitude of the fundamental peak and its harmonics change quite dramatically from sector to sector, as shown in Fig. 11. On occasions (sectors 8 and 9), the fundamental disappears altogether, resulting in a double-wave light curve.

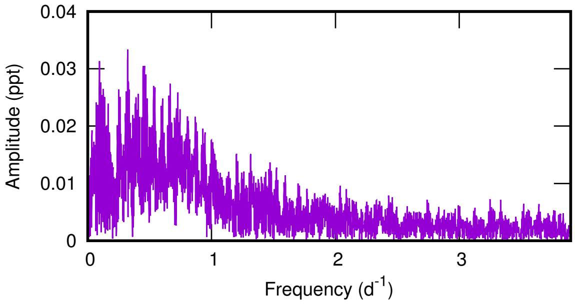

Figure 12. Periodogram of combined data for TIC 308748912.

4.10 TIC 308748912, HR 3217

This is a poorly studied B6V or B7IVek star with narrow lines ($v \sin i = 26\,\mathrm{km}^{-1}$; Zorec & Royer 2012). A study of the first two sectors from *TESS* by Balona et al. (2019) showed no significant periodicity The addition of four further sectors does not change this assessment (Fig. 12). While this star appears to be uninteresting, it presents an important challenge in understanding how mass loss can arise in a star which seems to lack any activity.

4.11 TIC 341040849, HIP 38433

This poorly-studied star is a member of NGC 2516. A peak at $1.406\,\mathrm{d}^{-1}$ and its harmonic are visible (Fig. 13). Both peaks are rather broad and variable in amplitude. This simple frequency spectrum is similar to that in TIC 55295028 (Fig. 3), κ Dra (Fig. 5) and TIC 279430029 (Fig. 11). The light curve is almost sinusoidal as in η Cen (Baade et al. 2016) and ν Pup (Baade et al. 2018a). Light curves showing a broad or very closely spaced multiple peaks and its harmonic are common and describe about 40 percent of the Be stars in our sample. They seem to be mostly mid- or late-B stars.

4.12 TIC 364398342, V374 Car

This star is a member of the open cluster NGC 2516 (Sampedro et al. 2017) and also an X-ray source (Naze & Motch 2018). From its position in the H-R diagram it can be classified as a blue straggler (Ahumada & Lapasset 2007) and may be a spectroscopic binary (González & Lapasset 2000). The star was discussed by Balona et al. (2019) but no periodicity was mentioned.

The time-frequency diagram and periodograms in Fig. 14 shows two broad peaks at about 1.25 and $2.50\,\mathrm{d}^{-1}$ as well as structure at very low frequencies. No resolved feature can be seen. Broad peaks such as these are found in several Be stars such as KIC 6954726 and KIC 11971405 (Rivinius et al. 2016b). It is possible that the broadening is simply a result of incoherence associated with co-rotating gas clouds close to the photosphere and that the $1.25\,\mathrm{d}^{-1}$ measures the approximate rotation frequency of the star.

4.13 TIC 425224332, β CMi

Saio et al. (2007) analysed photometry of β CMi from the

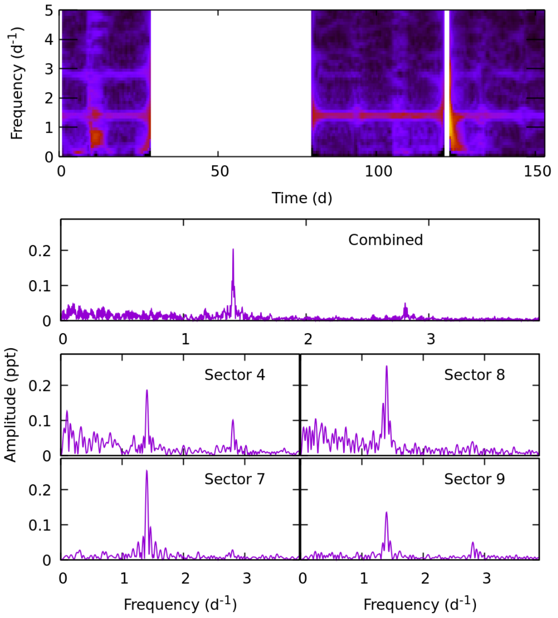

Figure 13. Time-frequency diagram and periodograms of the combined data and of individual observing sectors of TIC 341040849.

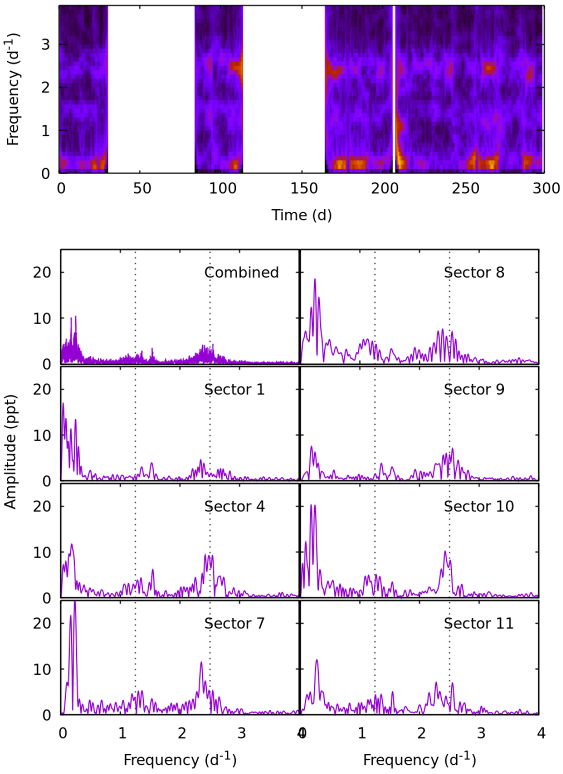

Figure 14. Time-frequency diagram and periodograms of the combined data and of individual observing sectors of TIC 364398342. The vertical dotted lines represent the frequency $\nu = 1.25\,\mathrm{d}^{-1}$ and its harmonic.

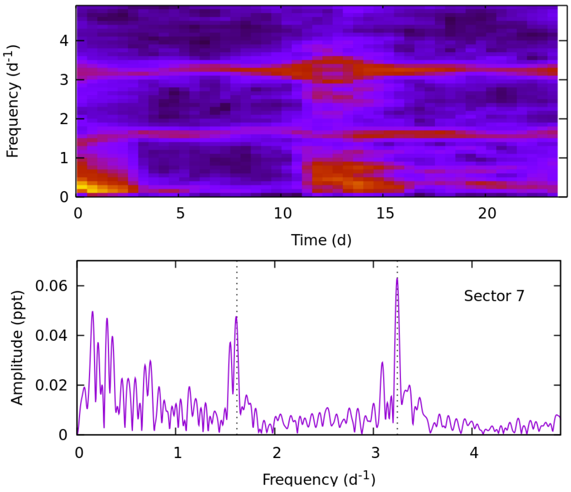

Figure 15. Time-frequency diagram and periodograms of β CMi. The dotted lines represent the assumed rotational frequency $1.621\,\mathrm{d}^{-1}$ and its first harmonic.

MOST satellite and concluded that it is a multiperiodic non-radial pulsator. In a re-analysis of the same data, Harmanec et al. (2019) did not find any coherent frequency. The dominant frequency of $3.257\,\mathrm{d}^{-1}$ appears to vary in frequency around its mean value. They conclude that there is only one stable frequency of $1.621\,\mathrm{d}^{-1}$ which they associate with the rotational frequency.

The *TESS* time-frequency diagram and periodogram is show in Fig. 15. The peak at around $1.61\,\mathrm{d}^{-1}$ is double, but this is due to slight frequency variations as can be seen by close inspection of the time-frequency diagram. The peak around $3.35\,\mathrm{d}^{-1}$ is equally variable in frequency and amplitude. There are indications of the 4th and 6th harmonics as well. Most likely, this is another case of a star in which the rotational frequency, $1.621\,\mathrm{d}^{-1}$, and its harmonic is present.

During the *MOST* observations, this frequency had very low amplitude and the light curve was dominated by the first harmonic, giving a double-wave variation. At that time, the first harmonic could have mistakenly taken as the rotational frequency. In the *TESS* data, the light curve has unequal minima so that the true rotation frequency is revealed.

5 DISCUSSION

In the Appendix periodograms of the remaining *TESS* Be stars are presented. Out of the 57 stars in our sample, 25 have somewhat broadened peaks or peaks with fine structure and at least one harmonic. In a further 18 stars the peaks are broad suggesting that they arise from circumstellar material. It is assumed that they are sufficiently close to the photosphere and co-rotate with the star. In this way approximate rotational frequencies for 43 stars (i.e. 75 percent of the sample) are listed in Table 1.

In most stars the fundamental is the dominant peak, but the first harmonic dominates in about one-third of the stars. This ratio may vary quite considerably from time to time, as is well known.

While it is always possible to attribute the quasi-

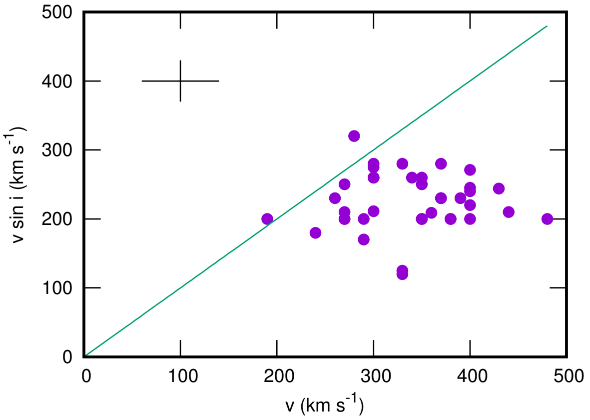

Figure 16. The projected rotational velocity, $v \sin i$, as a function of the equatorial rotational velocity, v, for the Be stars observed by *TESS*. The straight line represents $\sin i = 1$. Typical error bars for each point are shown by the cross.

periodic variations to NRP instead of rotational modulation, this would not advance the search for the mass-loss mechanism since it has been shown that Be stars rotate too slowly for NRP to be effective in this way (Zorec et al. 2016). A large fraction of non-Be stars also show rotational modulation and it is reasonable to suppose that Be stars are no different. However, the typical amplitude in Be stars (around 1000 ppm) is about an order of magnitude larger than in normal B stars (about 100 ppm; Balona 2019). This is in line with our hypothesis (described below) in which an active region ejects gas clouds. In the framework presented below, it is these co-rotating gas clouds which are responsible for the quasi-periodic light variations and not the active regions (associated with starspots) as in normal B stars.

If rotation is indeed responsible for the quasi-periodic light variations, then the equatorial rotational velocity, v, estimated from the photometric period and the radius should be related to the projected rotational velocity, $v \sin i$. A plot of $v \sin i$ as a function of v (Fig. 16) shows that this is indeed the case. Within the measured error, $v \sin i < v$ for all stars.

It should be noted that the error in v is considerable, as shown by the error bars in Fig. 16. Systematic errors in v are also likely to be present because the radius was derived from the effective temperature and luminosity. The derived effective temperatures for Be stars are not only poorly known, but probably somewhat cooler than the actual $T_{\rm eff}$ because it is mostly the gravity-darkened equatorial region that is observed. Thus the true radius is probably smaller than the estimated radius for the most rapidly rotating stars. Hence the estimated value of v for the more rapidly-rotating stars is likely to be too high. Another factor that would lead to a larger radius is multiplicity. Many stars are in unresolved multiple systems. While the *GAIA* parallax will be unaffected, the apparent brightness, and hence the derived luminosity and radius, will be larger than that of a single star. On the other hand, polar flattening due to rapid rotation means that the estimated equatorial radius, and hence v, is likely to be too low for the most rapidly rotating stars.

Not all Be stars exhibit rotational modulation. It is suspected that at times the photosphere is hidden from view. This is implied by the large change in apparent amplitude of the β Cep pulsations in the *CoRoT* light curve of TIC 234230792 (HD 49330) and possibly also in 27 CMa. The blanketing of the photosphere appears to be associated with an outburst. In very active stars, it might be the case that the presence of rotational modulation is masked.

The variable projected rotational velocity of Achernar (Rivinius et al. 2013) may be a result of gas clouds just above the photosphere. Depending on the latitude or height of these clouds, their velocity will vary and affect spectral line broadening.

On the assumption that rotational modulation is present in Be stars, we may suppose that active regions are present. This opens the way for a new hypothesis on the mass loss mechanism as proposed by Balona (2003) and outlined below.

6 THE MASS-LOSS MECHANISM

A strong clue to the nature of the Be phenomenon is the fact that a large proportion of these stars have, at times, double-wave light curves (strong first harmonic). In the NRP interpretation, this was taken as an indication of a preference for modes with $|m| = 2$. The tendency for the obscuration to be located on opposite sides of a star suggests the presence of a global dipole magnetic field (which needs only to have a strength of a few gauss to have a large effect on gas dynamics).

In the Sun and cool stars, flares are produced when magnetic field lines emanating from an active region reconnect. Until recently, stellar flares were generally found only on cool K and M dwarfs, but the *Kepler* mission has led to the realization that even more energetic flares (superflares) are to be found in normal F and G stars (Maehara et al. 2012) and on A stars as well (Balona 2012). It is thus conceivable that a flaring event could trigger mass loss in Be stars.

Mass loss due to flaring is a sudden event which describes Be outbursts rather well. The highly-ionized gas released in the process will expand and be trapped in closed magnetic loops. If we presume that the magnetic field configuration is an inclined dipole, gas will be confined to a torus inclined to the rotational axis and trapped at diametrically opposite regions where the magnetic equator intersects the stellar equator. This will account for the double-wave light curve in Be stars or, equivalently, the frequent occurrence of the first harmonic in the periodogram. The relative strength of the fundamental and first harmonic depends on the amount of gas trapped in the two diametrically opposite regions.

Gas will escape along open field lines and will be dragged and accelerated by the rapid rotation of the star. Depending on the rotational velocity, the gas will reach circular orbital speeds at some distance from the star if it is still ionized. After some time the gas, predominantly H and He, will cool down, become neutral (and thus unaffected by the magnetic field) and slowly dissipate into the inner circumstellar disk, rotating at Keplerian velocity.

In this model, whether a circumstellar disk is formed or not depends on two factors: (a) the presence of a tilted dipole magnetic field, (b) sufficiently rapid rotation to reach circular velocity while the gas is still ionized. In the intense radiation field of an early B star, the gas will remain ionized to large distances. Even if the star is rotating well below critical velocity, the long lever arm provided by the magnetic field will still ensure that the gas attains circular velocity while still ionized and under control of the magnetic field. This explains the wide range of rotational velocities in early B stars (Zorec et al. 2016).

On the other hand, the weak radiation field in a late B star limits the ionization radius closer to the photosphere. The lever arm is therefore shorter and requires a star already rotating close to critical for the gas to reach circular velocity while still ionized. This explains why late Be stars are rotating in a narrow band close to the critical rotation speed.

It is evident that the condition to attain circular velocity occurs in a far larger range of rotational velocities in early-type stars compared to late-type stars. This explains why most Be stars are of early type. Since the co-rotating ionized region is much larger in early B stars, it follows that activity will be higher in these stars. In this way one can understand why early B stars are more active than late Be stars.

7 CONCLUSIONS

It is clear that non-radial pulsation cannot be the trigger for mass loss because all studies have shown that Be stars rotate well below the required rotation rate. In the search for an alternative mass loss mechanism, we have examined light curves of 57 classical Be stars observed by the *TESS* satellite.

Analysis of these light curves shows that the fundamental and first harmonic can be identified in a large fraction (about 75 percent) of Be stars. Because starspots appear to be present in normal A and B stars (Balona et al. 2019), it is proposed that these regions may be the site of magnetic re-connection events which provide the required energy for driving mass loss with the assistance of rapid rotation. The ejected material, trapped in two diametrically opposite regions by a weak tilted dipole magnetic field, is presumed to be the origin of the light and line profile variations previously attributed to pulsation.

It is found that the most common light curve (about 40 percent) among Be stars is a simple single- or double-wave sinusoid. In the periodogram this appears as a slightly broadened peak, or peak with fine structure, and its first harmonic. The relative strengths of the first and second harmonics vary on a timescale of months to years. Stars showing this light curve morphology tend to be mid- to late-B stars.

In about 30 percent of Be stars, the periodogram still shows a fundamental and first harmonic, but with multiple peaks which form frequency groups. It seems that none of these multiple peaks are coherent since the appearance of the periodogram varies on timescales of months. These tend to be mostly mid- to early B stars.

In about 20 percent of Be stars, mostly of early type, the frequency groups merge to form regions of enhanced power (humps) in the periodogram, but fundamental and first harmonic can still be distinguished.

Finally in about 10 percent of Be stars, no obvious periodicity is visible and no frequency groups can be discerned.

For those stars where a fundamental and first harmonic can be identified in the periodogram, we have shown that the fundamental frequency is consistent with the expected rotational frequency.

It appears that during an outburst, much of the photosphere is obscured. This seems to be the simplest explanation for the rapid amplitude changes of β Cep pulsations in HD 49330 (Huat et al. 2009).

It is possible that the types of periodogram structure described above might be related to the amount of obscuration of the photosphere.

Be stars are clearly very complex and no doubt exhibit a huge range of physical processes. The study of the light curves, while important in providing constraints, cannot by itself provide sufficient information to reveal these processes. We present a model which attempts to provide a framework which may be expanded upon or rejected.

We still do not understand the connection between the quasi-periodic variations which occur close to the photosphere and the circumstellar disc. Further progress will require not only long-term photometric monitoring from space, but simultaneous spectroscopic observations as well.

ACKNOWLEDGMENTS

LAB wishes to thank the National Research Foundation of South Africa for financial support. Funding for the *TESS* mission is provided by the NASA Explorer Program. Funding for the *TESS* Asteroseismic Science Operations Centre is provided by the Danish National Research Foundation (Grant agreement no.: DNRF106), ESA PRODEX (PEA 4000119301) and Stellar Astrophysics Centre (SAC) at Aarhus University.

This work has made use of data from the European Space Agency (ESA) mission Gaia (`https://www.cosmos.esa.int/gaia`), processed by the Gaia Data Processing and Analysis Consortium (DPAC, `https://www.cosmos.esa.int/web/gaia/dpac/consortium`). Funding for the DPAC has been provided by national institutions, in particular the institutions participating in the Gaia Multilateral Agreement.

This research has made use of the SIMBAD database, operated at CDS, Strasbourg, France. The data presented in this paper were obtained from the Mikulski Archive for Space Telescopes (MAST). STScI is operated by the Association of Universities for Research in Astronomy, Inc., under NASA contract NAS5-2655.

REFERENCES

Ahumada J. A., Lapasset E., 2007, A&A, 463, 789
Arcos C., Kanaan S., Chávez J., Vanzi L., Araya I., Curé M., 2018, MNRAS, 474, 5287
Baade D., et al., 2016, A&A, 588, A56
Baade D., et al., 2018a, preprint, (`arXiv:1808.10254`)
Baade D., et al., 2018b, A&A, 610, A70
Baker R. H., 1920, Publications of the Astronomical Observatory of Michigan, 3, 29
Balona L. A., 1994, MNRAS, 268, 119
Balona L. A., 2003, in L. A. Balona, H. F. Henrichs, & R. Medupe ed., Astronomical Society of the Pacific Conference Series Vol. 305, Astronomical Society of the Pacific Conference Series. pp 263–+

Balona L. A., 2012, MNRAS, 423, 3420
Balona L. A., 2013, MNRAS, 431, 2240
Balona L. A., 2014, MNRAS, 439, 3453
Balona L. A., 2016, MNRAS, 457, 3724
Balona L. A., 2017, MNRAS, 467, 1830
Balona L. A., 2019, arXiv e-prints, p. arXiv:1910.01584
Balona L. A., Rozowsky J., 1991, MNRAS, 251, 66P
Balona L. A., Engelbrecht C. A., Marang F., 1987, MNRAS, 227, 123
Balona L. A., Sterken C., Manfroid J., 1991, MNRAS, 252, 93
Balona L. A., Cuypers J., Marang F., 1992, A&AS, 92, 533
Balona L. A., et al., 2016, MNRAS, 460, 1318
Balona L. A., et al., 2019, MNRAS, 485, 3457
Barrera L. H., Mennickent R. E., Vogt N., 1991, Ap&SS, 185, 79
Bernhard K., Otero S., Hümmerich S., Kaltcheva N., Paunzen E., Bohlsen T., 2018, MNRAS, 479, 2909
Bhattacharyya J. C., Ghosh K. K., 1989, IAU Circ., 4777, 3
Boashash B., ed. 2015, Time-Frequency Signal Analysis and Processing: A Comprehensive Reference UK : Academic Press
Bossi M., Guerrero G., Zanin F., 1993, A&A, 269, 343
Cameron C., et al., 2008, ApJ, 685, 489
Carrier F., Burki G., Richard C., 1999, A&A, 341, 469
Carrier F., Burki G., Burnet M., 2002, A&A, 385, 488
Chini R., Hoffmeister V. H., Nasseri A., Stahl O., Zinnecker H., 2012, MNRAS, 424, 1925
Cochetti Y. R., Arcos C., Kanaan S., Meilland A., Cidale L. S., Curé M., 2019, A&A, 621, A123
Cranmer S. R., 2005, ApJ, 634, 585
Cuypers J., Balona L. A., Marang F., 1989, A&AS, 81, 151
Domiciano de Souza A., Kervella P., Jankov S., Abe L., Vakili F., di Folco E., Paresce F., 2003, A&A, 407, L47
Domiciano de Souza A., et al., 2014, A&A, 569, A10
Eiroa C., et al., 2016, A&A, 594, L1
Gaia Collaboration et al., 2016, A&A, 595, A1
Gaia Collaboration Brown A. G. A., Vallenari A., Prusti T., de Bruijne J. H. J., Babusiaux C., Bailer-Jones C. A. L., 2018, preprint, (`arXiv:1804.09365`)
Ghosh K. K., Kuppuswamy K., Bhattacharyya J. C., 1989, IAU Circ., 4881, 3
Glebocki R., Gnacinski P., 2005, VizieR Online Data Catalog, 3244
Gontcharov G. A., 2017, Astronomy Letters, 43, 472
González J. F., Lapasset E., 2000, AJ, 119, 2296
Goss K. J. F., Karoff C., Chaplin W. J., Elsworth Y., Stevens I. R., 2011, MNRAS, 411, 162
Hahula M. E., Gies D. R., 1994, in Balona L. A., Henrichs H. F., Le Contel J. M., eds, IAU Symposium Vol. 162, Pulsation; Rotation; and Mass Loss in Early-Type Stars. p. 100
Harmanec P., et al., 2019, ApJ, 875, 13
Hill S. N., 1926, Publications of the Dominion Astrophysical Observatory Victoria, 3, 349
Houk N., Cowley A. P., 1975, University of Michigan Catalogue of two-dimensional spectral types for the HD stars. Volume I.
Huat A., et al., 2009, A&A, 506, 95
Jenkins J. M., et al., 2016, in Software and Cyberinfrastructure for Astronomy IV. p. 99133E, doi:10.1117/12.2233418
Juza K., Harmanec P., Hill G. M., Tarasov A. E., Matthews J. M., Tuominen I., Yang S., 1991, Bulletin of the Astronomical Institutes of Czechoslovakia, 42, 39
Kervella P., Domiciano de Souza A., Bendjoya P., 2008, A&A, 484, L13
Kilkenny D., Muller S., 1989, South African Astronomical Observatory Circular, 13, 69
Levenhagen R. S., Leister N. V., 2006, MNRAS, 371, 252
Lomb N. R., 1976, Ap&SS, 39, 447
Maehara H., et al., 2012, Nature, 485, 478
Maíz Apellániz J., et al., 2019, A&A, 626, A20
Mason B. D., Hartkopf W. I., Tokovinin A., 2010, AJ, 140, 735
Naze Y., Motch C., 2018, preprint, (`arXiv:1809.03341`)
Neiner C., et al., 2009, A&A, 506, 143
Neiner C., de Batz B., Cochard F., Floquet M., Mekkas A., Desnoux V., 2011, AJ, 142, 149
Oelkers R. J., et al., 2018, AJ, 155, 39
Ozuyar D., Caliskan S., Stevens I. R., Elmasli A., 2018, Publ. Astron. Soc. Australia, 35
Pavlovski K., Ruzic Z., 1990, A&A, 236, 393
Pecaut M. J., Mamajek E. E., 2013, ApJS, 208, 9
Peters G. J., Penrod G. D., 1988, in ESA Special Publication. pp 117–120
Peters G. J., Wang L., Gies D. R., Grundstrom E. D., 2016, ApJ, 828, 47
Porter J. M., Rivinius T., 2003, PASP, 115, 1153
Rivinius T., 2013, in Suárez J. C., Garrido R., Balona L. A., Christensen-Dalsgaard J., eds, Astrophysics and Space Science Proceedings Vol. 31, Stellar Pulsations: Impact of New Instrumentation and New Insights. p. 253 (`arXiv:1210.0784`), doi:10.1007/978-3-642-29630-7_46
Rivinius T., Baade D., Stefl S., Stahl O., Wolf B., Kaufer A., 1998, A&A, 333, 125
Rivinius T., Baade D., Štefl S., 2003, A&A, 411, 229
Rivinius T., Baade D., Townsend R. H. D., Carciofi A. C., Štefl S., 2013, A&A, 559, L4
Rivinius T., Townsend R. H. D., Baade D., Carciofi A. C., Leister N., Štefl S., 2016a, in Sigut T. A. A., Jones C. E., eds, Astronomical Society of the Pacific Conference Series Vol. 506, Bright Emissaries: Be Stars as Messengers of Star-Disk Physics. p. 17 (`arXiv:1602.03452`)
Rivinius T., Baade D., Carciofi A. C., 2016b, A&A, 593, A106
Saad S. M., et al., 2004, A&A, 419, 607
Saio H., et al., 2007, ApJ, 654, 544
Sampedro L., Dias W. S., Alfaro E. J., Monteiro H., Molino A., 2017, MNRAS, 470, 3937
Samus N. N., Kazarovets E. V., Durlevich O. V., Kireeva N. N., Pastukhova E. N., 2017, Astronomy Reports, 61, 80
Scargle J. D., 1982, ApJ, 263, 835
Semaan T., Hubert A. M., Zorec J., Gutiérrez-Soto J., Frémat Y., Martayan C., Fabregat J., Eggenberger P., 2018, A&A, 613, A70
Shokry A., et al., 2018, A&A, 609, A108
Silaj J., Landstreet J. D., 2014, A&A, 566, A132
Silva M. D. V., Napiwotzki R., 2011, MNRAS, 411, 2596
Slettebak A., 1979, Space Science Reviews, 23, 541
Spear G. G., Mills J., Snedden S. A., 1981, PASP, 93, 460
Stassun K. G., et al., 2018, AJ, 156, 102
Stefl S., Balona L. A., 1995, in Stobie R. S., Whitelock P. A., eds, Astronomical Society of the Pacific Conference Series Vol. 83, IAU Colloq. 155: Astrophysical Applications of Stellar Pulsation. p. 305
Tokovinin A., 2008, MNRAS, 389, 925
Tubbesing S., Rivinius T., Wolf B., Kaufer A., 2000, in Smith M. A., Henrichs H. F., Fabregat J., eds, Astronomical Society of the Pacific Conference Series Vol. 214, IAU Colloq. 175: The Be Phenomenon in Early-Type Stars. p. 232
Walker G. A. H., et al., 2005, ApJ, 635, L77
Wang L., Gies D. R., Peters G. J., 2018, ApJ, 853, 156
Zorec J., Royer F., 2012, A&A, 537, A120
Zorec J., et al., 2016, A&A, 595, A132

APPENDIX: NOTES ON ADDITIONAL STARS

In this section notes are given on stars not discussed in the main section. These stars were generally observed only in one sector. Periodograms are shown in Fig. A1. Where possible, the rotational frequency is estimated where a fundamental and its harmonic can be discerned in the periodogram. This might consist of a single peak and its harmonic, a broad peak and its harmonic or equally-spaced frequency groups each consisting of several peaks.

TIC 23037766, HR 2787: Balona et al. (1992) found possible light variations at 1.07 or 1.31 d^{-1} from ground-based photometry. The periodogram shows broad peaks at around 1.07 d^{-1} and its harmonic.

TIC 47296054, ϵ PsA: Balona et al. (2019) found a fundamental peak at 0.836 d^{-1}, assumed to be the rotational frequency, and three harmonics as well as an anomalous peak at 0.432 d^{-1} which is slightly different from half the fundamental frequency.

TIC 52665242, HR 2418: The fundamental peak at 1.1450(5) d^{-1} and three harmonics are visible.

TIC 53992511, HR 8408: Cuypers et al. (1989) found a frequency of 2.53 d^{-1} or half this value from ground-based photometry. The periodogram shows multiple peaks indicative of an SPB pulsator. The lines sit on top of broad features which are repeated every 1.6 d^{-1}. This is taken to be the rotational frequency.

TIC 56179720, 56 Eri: From ground-based photometry, Balona et al. (1992) found multiple peaks at around 0.9 d^{-1}. Later, Stefl & Balona (1995) derived a single photometric frequency of 0.80 d^{-1}. The periodogram shows a close doublet at 0.66 and 0.80 d^{-1} and a stronger peak at roughly double the frequency, 1.44 $^{-1}$. We take this to be a possible SPB variable.

TIC 67251066, λ Cyg: This is a known multiple system (Tokovinin 2008). The periodogram shows two broad peaks at about 1.1 and 2.2 d^{-1} which is assumed to be due to rotation.

TIC 71132174, DU Eri, HR 1423: Balona et al. (1992) found a frequency of 0.82 d^{-1} and its harmonic. The periodogram shows multiple peaks in three frequency ranges, 1.2–1.6, 2.4–3.2 and around 4.0 d^{-1}. The time-frequency diagram appears to show frequency drifts, so we interpret these three frequency groups as due to rotation at about 1.4 d^{-1}.

TIC 71727949, HR 2142: This star is a Be+sdO binary system with an orbital period of 80.913 d (Peters et al. 2016). Barrera et al. (1991) found a frequency of 1.26 d^{-1} from ground-based photometry. The main feature in the periodogram is a broad peak at 2.265 d^{-1} which is variable in amplitude, but no rotational frequency can be determined.

TIC 75047606, HR 3670: There is very little light variation in this star except for a low-amplitude peak at 1.6691(5) d^{-1} which we take to be the rotational frequency.

TIC 81584371, HR 2690, FV CMa: This is a close optical double with a brightness difference of 3.2 mag. Barrera et al. (1991) found a frequency of 1.92 d^{-1} from ground-based photometry. The periodogram is almost featureless apart from a low-amplitude broad peak at about 0.75 d^{-1} which is taken as the rotational frequency.

Table A1. Extracted frequencies, ν (d^{-1}), and amplitudes, A (ppt) for stars with high frequencies. The figures in brackets denote the error in the last digit.

ν	A	ν	A	ν	A
TIC 139385056:					
0.1727(6)	0.65(1)	6.0325(8)	0.45(1)	12.3253(9)	0.13(1)
1.1477(7)	0.53(1)	7.2484(7)	0.51(1)	12.6811(9)	0.09(1)
2.5689(8)	0.41(1)	7.8538(7)	0.49(1)	13.0979(9)	0.14(1)
3.6910(5)	0.86(1)	8.5140(2)	2.25(1)	13.3951(7)	0.54(1)
4.2221(8)	0.39(1)	8.9899(3)	2.40(1)	14.8955(9)	0.15(1)
4.4051(7)	0.59(1)	10.1424(9)	0.13(1)	15.1680(9)	0.09(1)
5.3059(9)	0.23(1)	10.8241(9)	0.31(1)	17.9759(9)	0.10(1)
5.9381(9)	0.35(1)	11.8906(9)	0.12(1)	22.3872(9)	0.09(1)
TIC 148316007:					
2.1640(4)	0.058(2)	7.7650(3)	0.082(2)	12.3314(9)	0.022(2)
2.5229(1)	0.238(2)	8.7062(5)	0.042(2)	13.2121(9)	0.021(2)
4.3382(5)	0.039(2)	9.8525(3)	0.081(2)	16.4693(9)	0.012(2)
4.5659(1)	0.242(2)	10.0119(1)	0.175(2)	16.5653(9)	0.013(2)
5.0403(1)	0.358(2)	10.8473(4)	0.050(2)	17.8625(9)	0.015(2)
6.7145(4)	0.045(2)	12.1613(4)	0.058(2)	18.5583(9)	0.015(2)
TIC 408382023:					
1.5481(2)	1.971(9)	5.8943(9)	0.155(5)	10.3183(9)	0.073(4)
3.0726(5)	0.653(7)	6.2010(7)	0.268(7)	13.9655(9)	0.114(5)
3.3370(9)	0.159(7)	6.9841(6)	0.358(7)		
TIC 409358619:					
1.8705(7)	0.193(5)	6.5570(9)	0.134(5)	11.5144(9)	0.106(5)
2.1763(9)	0.112(5)	7.9134(9)	0.119(5)	11.7959(9)	0.104(5)
2.3595(8)	0.152(5)	8.1915(9)	0.101(5)	12.3267(9)	0.118(5)
2.7678(2)	0.812(5)	8.7472(9)	0.087(5)	12.8563(9)	0.129(5)
3.0435(9)	0.134(5)	10.7575(9)	0.107(5)	14.7442(9)	0.091(5)
5.7636(7)	0.174(5)	10.9339(7)	0.191(5)		
TIC 443616529:					
1.1342(5)	1.03(1)	5.6259(8)	0.50(1)	8.8468(8)	0.78(1)
2.9881(8)	0.52(1)	6.0771(8)	0.67(1)	8.9063(5)	0.91(1)
3.3846(7)	0.74(1)	6.4739(2)	5.25(1)	12.1254(9)	0.18(1)
4.9365(8)	0.51(1)	6.8711(9)	0.41(1)	13.2080(9)	0.28(1)
5.0159(7)	0.53(1)	7.6464(9)	0.36(1)		

TIC 99115271, HR 7789: The periodogram shows two peaks at 0.529 d^{-1}, which we assume is the rotational frequency, and its harmonic.

TIC 120967488, HR 7262: The periodogram shows three broad structures at frequencies 1.0, 2.0 and 4.0 d^{-1} which is assumed to be a result of rotation.

TIC 139385056, HR 2855, FY CMa: The periodogram shows high frequencies typical of a β Cep pulsator, but no indication of a rotational peak. Table A1 lists the most significant extracted frequencies.

TIC 139472176, HIP 11116: The periodogram shows just a single peak at 0.7727(8) d^{-1}, assumed to be rotation, and several harmonics.

TIC 140214221, HR 1956, α Col: A peak at 0.9258(1) d^{-1} and its harmonic is taken as rotation.

TIC 144028101, HR 5683, μ Lup: A low-amplitude peak at 33.156(3) d^{-1}, amplitude 0.16(2) ppt, might be due to a δ Sct companion, but we classify it as a Maia variable. No other significant period is present.

TIC 148316007, HR 2507: There is a large number of peaks in the range 2–20 d^{-1} indicating that this is a β Cep star (Table A1). A broad peak at 2.523 d^{-1} and its harmonic is taken to be the rotational frequency. The star lies somewhat below the zero-age main sequence.

TIC 151300497, HR 6397: This is a double-lined spectroscopic binary, with no significant variability.

TIC 159117671, HR 4893: The periodogram shows five peaks with frequencies which may be represented by a fre-

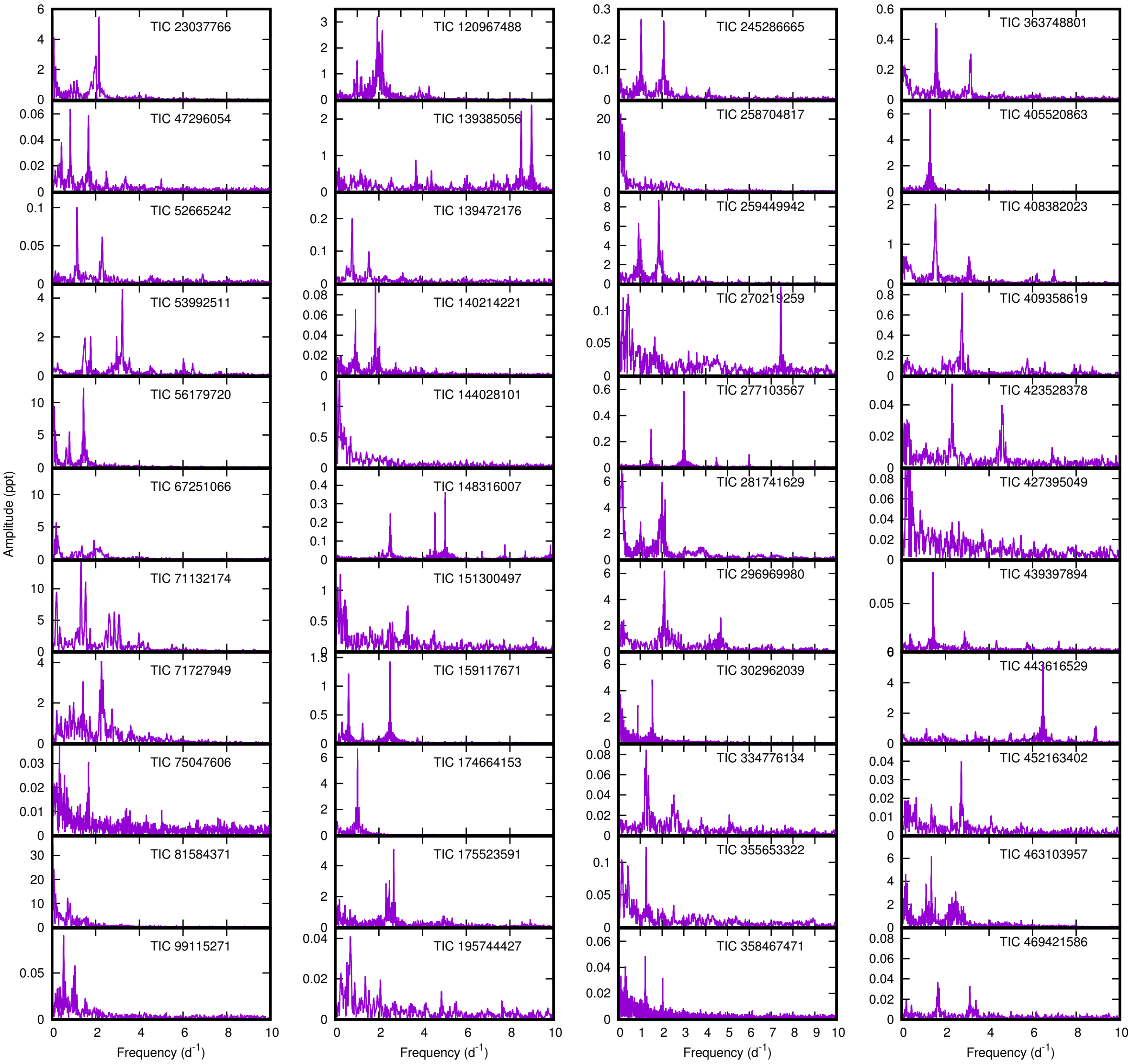

Figure A1. Periodograms of stars not discussed in the main section.

quency 0.3058 d^{-1} and its harmonic and 1.2522 d^{-1} and its first two harmonics. The latter is assumed to be the rotational frequency. The lower frequency, which corresponds to a period of 3.27 d, may be of orbital nature. The star is in a multiple system with one of the components being a spectroscopic binary with a period of 3.2866 d (Tokovinin 2008).

TIC 174664153, HR 2968: This is a member of the open cluster NGC 2451B. The star appears to be a binary in an eccentric orbit with a period of 371 d (Carrier et al. 1999). There is only one significant peak in the periodogram at 1.01853(7) d^{-1} which we take to be rotation.

TIC 175523591, HR 3022: This star is classified as an eclipsing binary in the *General Catalogue of Variable Stars*, but no period is given. No eclipses are visible in the *TESS* data. The periodogram shows at least two groups at around 2.5 d^{-1} and its harmonic. The first group comprises three distinct peaks at 2.674, 2.480 and 2.321 d^{-1}, but with amplitude variations, The mean frequency of about 2.5 d^{-1} is taken as the rotational frequency.

TIC 195744427, HR 8028, ν Cyg: There are no distinctive features in the periodogram except a low-amplitude peak at about 0.69 d^{-1}.

TIC 245286665, HR 7719: The periodogram shows a presumed rotational frequency at 1.0393(3) d^{-1} and three harmonics.

TIC 258704817, HR 5500: This is a double-line spectroscopic binary (Chini et al. 2012). The periodogram does not show any distinctive features.

TIC 259449942, HR 2921: This star, a member of the open cluster NGC 2422, contains a sdO companion in a long-period orbit (Wang et al. 2018). The periodogram shows a broad peak at 1.1 d^{-1},assumed to be the rotational frequency, and several harmonics.

TIC 270219259, η PsA: The star is a close double with a brightness difference of 1.09 mag. Balona et al. (2019) found broad low-frequency features at around 1.7 d^{-1} for part of the time. The most interesting feature in the periodogram is a sharp peak at 7.4450(7) d^{-1} (amplitude 0.139(5) ppt) which must be due to pulsation. We classify it as a Maia variable.

TIC 277103567, 29 Dor: From an analysis of ground-based and Hipparcos photometry, a very-low amplitude variation with a period of 395.48 d was determined. It was later confirmed from radial velocity measurements (Carrier et al. 2002). Balona et al. (2019) found a peak at 1.496 d^{-1} and three harmonics. This is confirmed with the additional *TESS* data where a peak at 1.49668(3) d^{-1}, assumed to be the rotational frequency, and at least three harmonics are visible.

TIC 281741629, JL 212, BG Phe: This is a high Galactic latitude runaway Be star. No periodicity was found from the first two *TESS* sectors (Balona et al. 2019) and no further data are available. The possible subdwarf classification is due to Kilkenny & Muller (1989). The luminosity determined from the *Gaia* parallax places this star at the end of core hydrogen burning, so it cannot be a subdwarf.

TIC 296969980, θ Cir: This is a double-line spectroscopic binary (Chini et al. 2012) and an interferometric double with an orbital period of 39.61 yr (Mason et al. 2010). The periodogram consists of two peaks at 2.1047(2) and 4.6893(5) d^{-1} on top of broad features. We classify it as SPB, but no rotational frequency can be determined.

TIC 302962039, HR 3642: The periodogram features two sharp peaks at 1.5463(3) and 0.8875(3) d^{-1}. The light curve shows irregular variations with a timescale of about 40 d. No rotational frequency can be determined.

TIC 334776134, HR 4123: A broad peak at about 1.3 d^{-1} and three harmonics are visible. We presume this to be rotation.

TIC 355653322, ϵ Tuc: Balona et al. (2019) found a low-amplitude peak at 1.2659(6) d^{-1} and its harmonic. This is assumed to be the rotation period.

TIC 358467471, HIP 38779: This star is a member of NGC 2516. Two unrelated peaks are visible at 1.2278(1) d^{-1} and 2.0282(1) d^{-1}. No rotation peak can be identified.

TIC 363748801, η1 TrA: The periodogram shows peaks at 1.5548(3) d^{-1} (assumed to be the rotational frequency) and at least one harmonic.

TIC 405520863, 39 Cru, HR 4823: Balona et al. (1992) found a frequency of 1.295 d^{-1} from ground-based photometry. The periodogram shows the same frequency, 1.2982(2) d^{-1}, which is assumed to be due to rotation. The 1st and 2nd harmonics are barely visible.

TIC 408382023, HR 3858: A broad peak at 1.55 d^{-1}, assumed to be the rotational frequency, and two harmonics are visible. In addition, some low-amplitude peaks between 5–13 d^{-1} (Table A1) suggest that this is a Maia variable.

TIC 409358619, HR 5316: There are multiple peaks in the periodogram up to about 13 d^{-1}, indicating a β Cep star. Extracted frequencies are listed in Table A1. The first harmonic of the highest-amplitude peak at 2.7678 d^{-1} is faintly visible. We assume this might be the rotational frequency.

TIC 423528378, ζ Crv, HR 4696: Barrera et al. (1991) found a photometric frequency of 1.96 d^{-1}. The periodogram shows a broad peak at 2.306(1) d^{-1}, assumed to be due to rotation, as well as the 1st and 2nd harmonics.

TIC 427395049, θ2 Ori, HR 1897: This star is a double-line spectroscopic binary (O9.2V+B0.5V(n)) in a very rich field (Maíz Apellániz et al. 2019). No clear periodicity is visible in the periodogram.

TIC 439397894, 2 Cet, HR 9098: A peak at 1.4408(3) d^{-1}, assumed to be the rotational frequency, and as many as 5 harmonics are visible. In addition, there is a much weaker peak at 0.357(2) d^{-1} and some harmonics which may perhaps be orbital in nature.

TIC 443616529, ϕ Leo: Evaporation of solid, comet-like bodies grazing or falling into the star has been proposed as the source of variable spectral lines (Eiroa et al. 2016). This is a δ Sct variable with several peaks (Table A1).

TIC 452163402, A Cen, HR 4460: The strongest peak in the periodogram is at 2.7323(7) d^{-1}, but the sub-harmonic at 1.364(2) d^{-1} is present with a very low amplitude. This is assumed to be the rotational frequency.

TIC 463103957, HR 4009: A broad peak at 1.36 d^{-1} and its harmonic is taken as the rotation frequency.

TIC 469421586, HR 7843: This is a multiple system. A broad peak at 1.66 d^{-1} and its harmonic is taken as the rotational frequency. In addition, two peaks at 37.1229(5) and 41.574(2) d^{-1} (amplitudes 0.078(2) and 0.019(2) ppt respectively) suggest that it is a Maia variable or contains a δ Sct companion.